Between Scylla and Charybdis: Hydrophobic Graphene-Guided Water Diffusion on Hydrophilic Substrates

Jin-Soo Kim[1], Jin Sik Choi[1], Mi Jung Lee[2], Bae Ho Park[2,*], Danil Bukhvalov[3], Young-Woo Son[3], Duhee Yoon[4], Hyeonsik Cheong[5], Jun-Nyeong Yun[6], Yousung Jung[6], Jeong Young Park[6,**], and Miquel Salmeron[7]

[1]Creative Research Center for Graphene Electronics, Electronics and Telecommunications Research Institute (ETRI), Daejeon 305-700, Korea.

[2]Division of Quantum Phases and Devices, Department of Physics, Konkuk University, Seoul 143-701, Korea.

[3]Korea Institute for Advanced Study, Seoul 130-722, Korea.

[4]Electrical Engineering Division, Cambridge University, Cambridge, CB3 0FA, UK

[5]Department of Physics, Sogang University, Seoul 121-742, Korea.

[6]Graduate School of EEWS, NanoCentury KI, Korea Advanced Institute of Science and Technology (KAIST), Daejeon 305-701, Korea.

[7]Materials Science Division, Lawrence Berkeley National Laboratory, Berkeley, CA 94720, USA.

[*]email: baehpark@konkuk.ac.kr; **email: jeongypark@kaist.ac.kr

The structure of water confined in nanometer-sized cavities is important because, at this scale, a large fraction of the hydrogen bonds can be perturbed by interaction with the confining walls. Unusual fluidity properties can thus be expected in the narrow pores, leading to new phenomena like the enhanced fluidity reported in carbon nanotubes. Crystalline mica and amorphous silicon dioxide are hydrophilic substrates that strongly adsorb water. Graphene, on the other hand, interacts weakly with water. This presents the question as to what determines the structure and diffusivity of water when intercalated between hydrophilic substrates and hydrophobic graphene. Using atomic force microscopy, we have found that while the hydrophilic substrates determine the structure of water near its surface, graphene guides its diffusion, favouring growth of intercalated water domains along the C-C bond zigzag direction. Molecular dynamics and density functional calculations are provided to help understand the highly anisotropic water stripe patterns observed.

Confined water attracts significant interest because of its ubiquity in common phenomena, such as fluid flow and lubrication[1, 2, 3, 4]. In spite of this, a molecular-level understanding of water structure and dynamics near the confining boundaries is lacking[5, 6] and yet it is fundamental to understand the biological functionality of proteins and membranes, the wettability of surfaces, and boundary slippage conditions, which are of particular interest today in the emerging area of nanofluidic science. Because the water structure is likely to be perturbed significantly near interfaces, new properties can be expected in extreme confinement. It has been reported, for example, that water exhibits exceptional diffusion properties inside hydrophobic carbon nanotubes (CNT) via fast ballistic motion[7] and unexpected phases, depending on the diameter of the CNT[8]. An active discussion is ongoing about these observations, with conflicting reports as different techniques and calculation methods are used[9, 10, 11, 12].

Here, we report the results of our study on the intercalation and diffusion of water between graphene and hydrophilic substrates using atomic force microscopy (AFM), a technique that provides information about the crystallographic orientation of the confining surfaces. These materials, at opposite ends of interaction strength, one hydrophobic and the other hydrophilic, provide a unique laboratory to study the structure of confined water, its intercalation, and diffusion[13, 14, 15, 16]. As we will show, the opposite affinities of these two surfaces for water give rise to competition between the tendency to order induced by the mica and diffusion along the slippery directions induced by graphene.

Results

Figure 1(a) shows an AFM topographic image of graphene flakes deposited on hydrophilic and single-crystalline mica (GM). In this image, monolayer, bi-layer, and few-layer graphene flakes can be observed, with boundaries marked by red, blue, and white lines, respectively. As in previous work[17], we find that water intercalates between the graphene and mica, forming a flat layer that fills most of the interior of the first graphene monolayer, except for a narrow region with jagged boundaries 200–300 nm wide from the graphene edge. Figure 1(b) shows the height profile obtained along the white dashed arrow in Fig. 1(a). The height of the first graphene monolayer over the mica substrate in the dry edge region is 0.28 ± 0.06 nm,

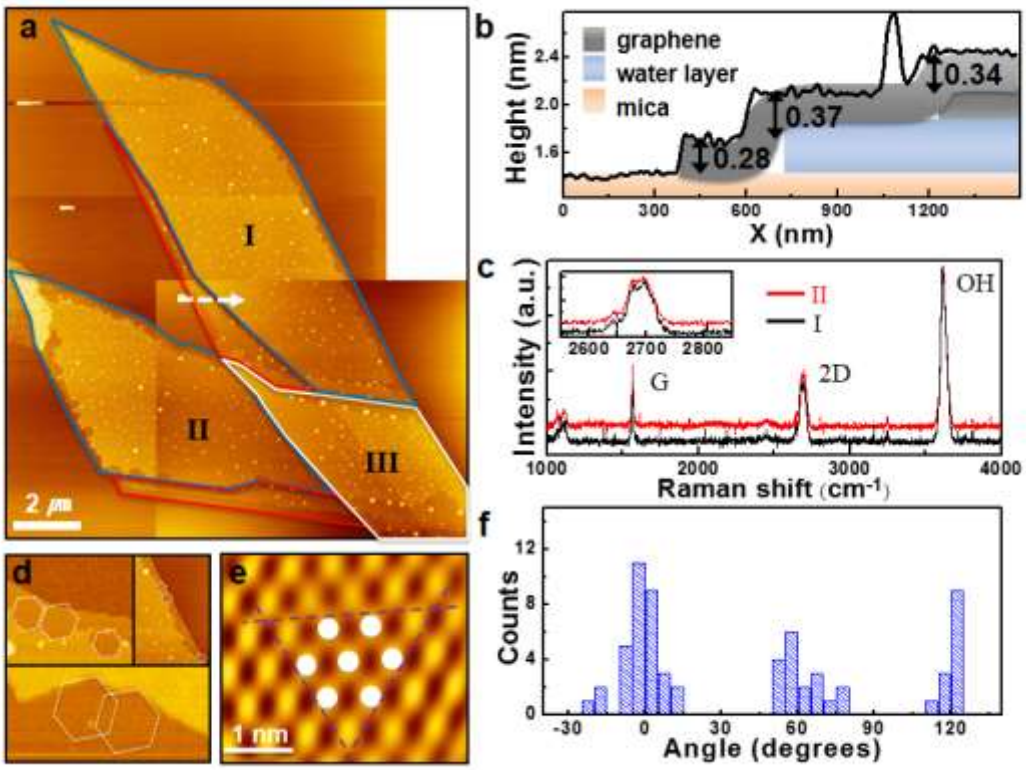

Figure 1. Water intercalated between graphene and mica. (**a**) AFM topographic image of graphene flakes deposited on mica at 30–40% RH using the mechanical exfoliation method. Red, blue, and white lines have been drawn around the flake contours to indicate monolayer, bilayer, and few-layer graphene, respectively. (**b)** Height profile obtained along the dashed white arrow in (**a**). The first (0.28 ± 0.06 nm), second (0.37 ± 0.04 nm), and third (0.34 ± 0.04 nm) steps correspond to the thicknesses of the monolayer graphene directly on the mica substrate, the ice monolayer intercalated between the mica and the monolayer graphene, and the second graphene layer, respectively. Notice that the confined water film boundaries have receded from those of the graphene flake. (**c**) Spatially-resolved Raman spectra of the graphene bilayer regions I and II in (**a**). The inset shows expanded Raman spectra near the 2D peak position. (**d**) Selected AFM images of boundary regions where the water edges follow well-defined hexagonal shapes. (**e**) Low-pass filtered stick-slip image obtained on the mica surface. White circles indicate hollow sites in the hexagonal structure. The distances between the circles are 0.55 ± 0.06 nm, which are comparable to the in-plane lattice constant of mica (0.52 nm). The purple dashed lines are the crystallographic orientations of the mica surface. (**f**) Statistics for the orientation of the edges in (**d**) with respect to the near-horizontal purple dashed line in (**e**).

which is smaller than the layer spacing in graphite (0.34 nm). This value is also lower than those previously reported (0.4 ~ 0.9 nm)[17, 18, 19]. A second step, with a height of 0.37 nm, appears at the boundary of the water layer[17]. This height is similar to the spacing between the basal planes of I_h ice.

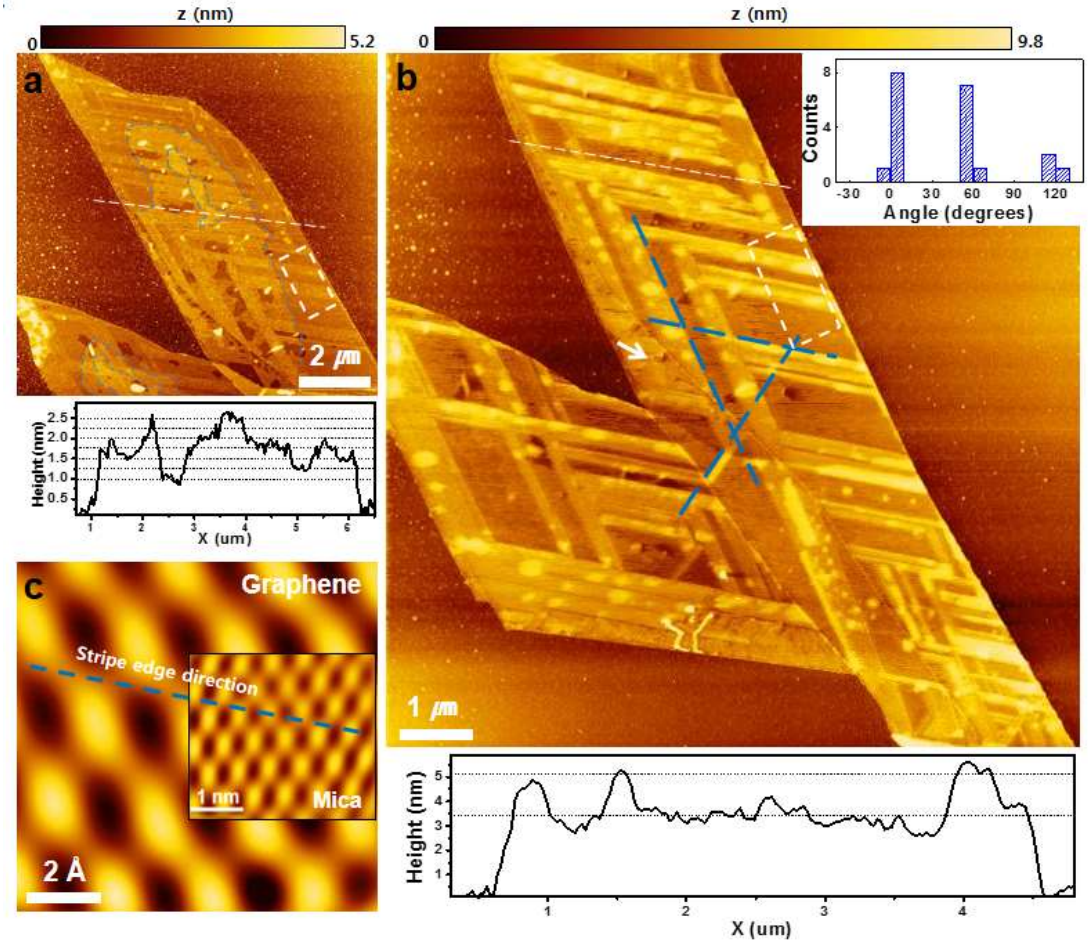

Figure 2. Water diffused inbetween graphene and mica. AFM topographic images obtained (**a**) after one week of exposure to high RH (>50%) and (**b**) after exposure to similar high RH for one additional week. The height profiles below (**a**) and (**b**) were obtained along the white dashed lines in (**a**) and (**b**), respectively. The blue contour lines in (**a**) denote the edges of layered water structures and blue dashed lines in (**b**) delineate the directions of the stripe patterns, which form angles of ~ 60° with each other. (**c**) Low-pass filtered stick-slip image of graphene measured in the region denoted by the white arrow in (**b**). The inset in (**c**) shows a low-pass filtered stick-slip image of mica duplicated from Fig. 1(e). The blue, dashed line in (**c**) is copied from the near-horizontal direction of stripe patterns in (**b**). The inset in (**b**) shows the distribution of the relative angle of the stripe patterns with respect to one zigzag direction of graphene in (**c**).

The boundaries of the intercalated water film under the graphene are jagged, with sides forming angles of approximately 120°, as visualized by the white hexagons in Fig. 1(d), corresponding to selected images of the water layer edges from Fig. 1(a). These sides are compared to the lattice directions of the mica that could be obtained using friction force microscopy[20]. They are aligned with the compact lattice directions of the mica surface, shown

by the dashed lines in the low-pass filtered stick-slip image of Fig. 1(e). Figure 1(f) shows statistics of the angles between the water layer edges and the lattice direction of the mica, with reference to the near-horizontal dashed line in Fig. 1(e). This orientation preference of water agrees with a previous literature report[21] and supports the notion that water intercalated between the graphene and mica forms an ice-like layer. On the other hand, intercalation of water under exfoliated graphene on a hydrophilic, amorphous SiO_2 substrate (GS) does not show crystalline features under similar humidity conditions (Supplementary Fig. S1).

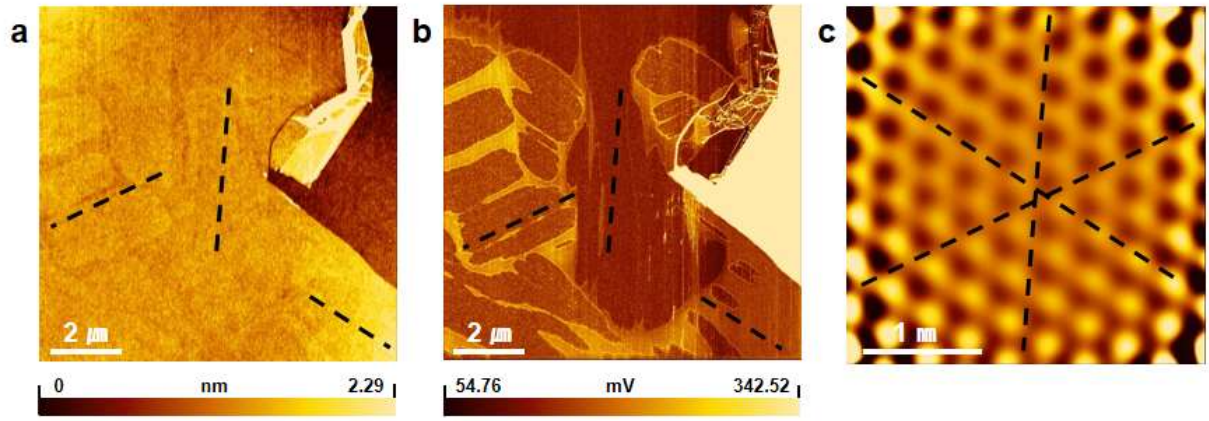

Figure 3. Water diffusion guided by graphene on SiO_2. (**a**) AFM topographic image and (**b**) simultaneously-obtained friction image of graphene on a SiO_2 substrate under high RH (~60%). (**c**) Low-pass filtered stick-slip image obtained on the graphene. Black dashed lines indicate the zigzag directions of the graphene, which are determined in (**c**).

To study the intercalation pathways of water, we exposed the GM sample to high relative humidity (RH) for one week (>50% RH). The topographic image in Fig. 2(a) obtained after this exposure shows new layered structures (irregular shapes denoted by the blue contour lines), and stripe-like structures (narrow strait segments), formed by intercalation of additional water. We confirmed that water intercalation occurred at the interface between the mica and graphene and not between the graphene layers, since no changes in the Raman peaks of graphene were observed, except for an increase in the O-H peak (Supplementary Fig. S2). The layered structures, with various thicknesses, have been frequently observed when graphene is deposited on mica at high humidity (RH ~ 90%)[17]. The height of a layered structure is ~0.25 nm according to the height profile measured along the white dashed line in Fig. 2(a). The water stripes in the white dashed rectangle of Fig. 2(a) have an average height of 0.34 nm, which is similar to the height of the hexagonal waterlayer[22, 23]. Additional exposure to high humidity (~50% RH) for another week increases the stripe thickness to 1.23

~ 1.49 nm, which corresponds to 3 or 4 layers (white dashed rectangle in Fig. 2(b) and height profile below Fig. 2(b)). At the same time, the layered structure disappears almost completely. There are two important observations from these experiments: one is that the stripe patterns grow in three well-defined directions, forming angles of ~ 60˚ with each other (blue dashed lines in Fig. 2(b)); the other is that the growth in thickness of the stripes implies poor wetting beyond the first layer.

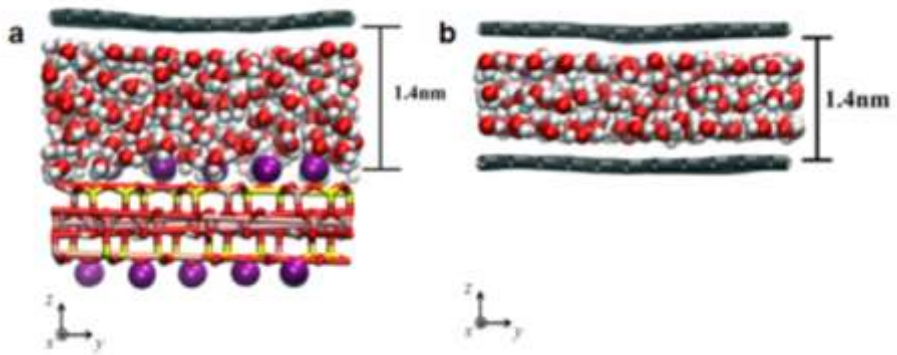

Figure 4. **Atomic model of molecular dynamics (MD) simulation.** Snapshots of MD simulations for water molecules (**a**) between graphene and mica and (**b**) between graphene and graphene. The mica structure is a 2:1 layer-type dioctahedral aluminosilicate with the muscovite formula $K_2Al_4(Al_2Si_6)O_{20}(OH)_4$. Colour codes used: potassium (purple), silicon (yellow), aluminium (pink), oxygen (red), and hydrogen (white).

To investigate the correlation between the water stripe structure and that of mica and graphene, we compared the stripe orientation with the lattices of these two materials, which we obtained from the stick-slip (friction) images, as shown in Figs. 1(e) and 2(c). As can be seen, the stripe orientation (marked by the dashed blue line) coincides with the C-C zigzag directions of graphene. The distribution of the measured angles between one zigzag direction of graphene and the water stripes is very narrow, with peak counts near 0°, 60°, and 120°, as shown in the inset of Fig. 2(b). Although the atomic lattice of graphene in Fig. 2(c) is that of the upper layer of the bi-layer graphene, the zigzag direction of the upper graphene layer is the same as the lower one (Supplementary Fig. S3). It should be noted that the mica and graphene lattice directions in these experiment differ by 15°.

To examine whether the water stripe pattern is only guided by the graphene overlayer, we carried out similar water diffusion experiments for a GS sample at a RH of ~ 60%. As shown in the contact topographic AFM image in Fig. 3(a), the graphene has bulging regions due to water intercalation. These regions show a lower friction (Fig. 3(b)), indicating that the

intercalated water acts as a subsurface lubricant[24]. As shown from the lattice-resolved stick-slip image of graphene in Fig. 3(c), the edges of the water domains also follow the zigzag directions of graphene. These indicate that the growth of the water patterns is guided by the crystallographic orientation of the graphene overlayer and not by the strongly-binding hydrophilic substrate.

The observations can be summarized as follows. The structure of the first intercalated water layer is strongly dependent on the structure of the hydrophilic substrates, which, in the case of mica, is crystalline and epitaxially oriented. When more water intercalates between the graphene and the substrate, additional water appears to not wet the first water layer, resulting in the formation of multilayer stripes, a phenomenon theoretically described by Wang [25]. The water stripes are elongated with the long edge in the direction of the C-C atomic zigzag chains of graphene. The dewetting of the water stripe pattern was confirmed by environment control (Supplementary Fig. S4).

Discussions

Modeling and calculations can provide insights into the formation and alignment of the water stripe patterns after exposure to high humidity. Since the water stripes have widths on the order of micrometers, their internal structure is not necessarily determined by the orientation and dynamics of their edges. To simulate the flow of water with stripe patterns underneath the graphene, we performed molecular dynamics (MD) simulations on water layers at 300K. The simulation box is similar to the experimental configuration shown in Fig. 4(a), where water molecules are sandwiched between the graphene and mica surfaces separated by 1.4 nm. Diffusivity of this nano-confined water as well as that of water between two mica surfaces is reduced roughly by a factor of 2 compared to bulk water, consistent with previous MD simulations[26] (Supplementary Table I). The differential water diffusivity projected along the zigzag (D_z) vs. armchair (D_a) directions was then calculated after 10 ns equilibrium simulations. We observe a 40% enhancement in water diffusivity along the zigzag direction, compared to the armchair direction. Since both graphene and mica surfaces have six-fold symmetry with directional anisotropy, we considered an additional two model systems: one with only graphene surfaces (Fig. 4(b)) and the other with only mica surfaces (Supplementary Fig. S5(a)). When water molecules are confined between two graphene surfaces, instead of

one graphene and one mica, the relative diffusivity D_z/D_a increases from 1.4 to 3.9, while the diffusion becomes almost 2D-isotropic when the confining surfaces are both mica. On the basis of these results, the primary role of the hydrophilic mica surfaces in the hydrophilic/hydrophobic amphiphilic interface seems to be to anchor the water layer in crystallographic commensurability with its lattice. The directional diffusion of water, however, is controlled by the graphene surface. A related system that would more dramatically reflect the different diffusional behavior of water along different chirality of the graphitic surfaces would be CNT filled with water due to the increased number of interfacial water molecules. Thus, we performed MD simulations for the water-filled (16,16) and (28,0) CNT 2.1 nm in diameter (Supplementary Fig. S5(b)). We obtained a similar 4.5-fold increase in water diffusivity along the zigzag flow direction, as compared to the armchair direction, consistent with the present experimental observations with the graphene surface guiding the water flow.

These MD simulation results can be understood more clearly by performing first-principles calculations on the potential energy surfaces of water on graphene. The mica substrate is simply regarded as a confining wall in the present calculations of the activation barrier. We found that two ice layers underneath the graphene form a hexagonal-like structure with a crystallographic orientation that coincides with one of graphene, being similar to the water structure without mica[27]. From the atomic models projected along the graphene zigzag direction (Supplementary Fig. S6(a)) and along the armchair direction (Supplementary Fig. S6(b)), we can see that the inter-ice layer interactions are anisotropic. We calculated the total energy changes of the system when the ice layer nearest to graphene slides along various directions, with all other parameter systems remaining the same. As expected from the local hydrogen bonding structures, the energy barrier for sliding is highly anisotropic, where the energy barrier for sliding along the armchair direction (~1.7 eV) is three times higher than that (~0.6 eV) along the zigzag direction. In addition, we confirmed that this anisotropy in the energy barrier was enhanced by the confining effect of the mica substrate (see Supplementary Fig. S6 for more details). These results are consistent with the potential energy surfaces for a water molecule inside CNTs of different chirality but similar diameter where the lower activation barrier and thus faster water dynamics were observed for water inside the (16,16) CNT with the zigzag flow direction[28].

In conclusion, we have discovered new wetting and diffusion phenomena of water when confined between surfaces of opposite affinity, one hydrophilic and the other hydrophobic. The hydrophilic surface strongly anchors the first water to form a uniform monolayer film. Additional water intercalates to form multilayers with poor wetting characteristics, a phenomenon due to the hydrophobic surface. In addition, the hydrophobic surface determines the diffusion pathways of water along the zigzag directions of graphene. Our model and calculations provide a rationale for these observations: the energy barrier increases for directions away from the optimal zigzag. This should further stimulate fundamental studies of boundary slippage, both theoretically and experimentally, because such strong-weak mixed interactions of fluids with confining layers are prevalent in nature, particularly in biological and environmental phenomena, rock weathering and flow, etc.

METHODS

Specimen preparation. Graphene sheets were prepared via the standard mechanical exfoliation method using Kish graphite flakes on the surface of cleaved muscovite mica and SiO_2 substrate at ambient relative humidity (RH) ranging from 30% to 40% without further treatment. The thin graphene samples were sorted using optical microscopy. A high-humidity treatment was carried out, with the sample surrounded by, but not contacting, ultrapure water with a specific resistivity > 18 Mohm·cm in a sealed polyester bag. The humidity in the sealed polyester bag increased logarithmically with time and reached ~ 90% after one week.

AFM experiments. Topographic and friction AFM images were obtained using tapping and contact modes, respectively, with a Seiko SPA-300HV AFM. We used diamond-like carbon tips with a typical curvature radius of 1 nm (NSG01_DLC from NT-MDT) to get topographic, phase, and stick-slip images, and lateral friction tips (PPP-LFMR with a spring constant of 0.2 N/m from Nanosensors) to get topographic and friction images at ambient conditions. We used Pt-coated silicon AFM tips with a tip radius less than 25 nm (PPP-NCHPt from Nanosensors) to simultaneously get topographic and phase images at low temperature and pressure. The topographic images were processed with line- and plane-subtraction corrections to compensate for scanning drift. Low-pressure measurements were performed in the AFM chamber evacuated to 10^{-3} Torr by means of a JANIS turbo-pumping station (TP-75-DR). The temperature in the AFM vacuum chamber was controlled using a built-in temperature controller (model E5CN from OMRON electronics). The height distributions of the water

stripe patterns were obtained using Gwyddion scanning probe microscopy data analysis software (http://gwyddion.net/).

Raman experiments. For the micro-Raman measurements, the 514.5-nm line of an Ar ion laser was used as the excitation source. The laser beam was focused onto the graphene sample by a 40X microscope objective lens. The spatial resolution was less than 1 μm, and the spectral resolution was about 1 cm^{-1}.

MD simulations. The water-carbon interactions were modelled using Lennard-Jones 12-6 potentials $E^{LJ12-6} = 4\varepsilon\{\left(\frac{\sigma}{r}\right)^{-12} - \left(\frac{\sigma}{r}\right)^{-6}\}$, where $\varepsilon_{C\text{-}H}$ =0.0318 kcal/mol, $\varepsilon_{C\text{-}O}$ = 0.113 kcal/mol, $\sigma_{C\text{-}C}$ = 3.39 A, $\sigma_{O\text{-}O}$ = 3.17 A, $\sigma_{C\text{-}H}$ = 2.80 A, $\sigma_{C\text{-}O}$ = 2.95 A[7]. The interactions between water and the mica structure were obtained by the Lorentz-Berthelot combination rules, $\varepsilon_{ab} = \sqrt{\varepsilon_a \varepsilon_b}$ and $\sigma_{ab} = \frac{\sigma_a + \sigma_b}{2}$. The force field parameter for the mica structure was taken from ref. 29. The extended simple point charge (SPC/E) water model was used. To test the sensitivity of our computed diffusivity results to force field parameters, we repeated our simulations using the TIP3P water model widely used in CNT-water systems and found quantitatively similar results within 10 % error. A simulation box with dimensions 2.7 x 2.7 x 1.4 nm^3 containing 270 ± 30 water molecules was used. The confined water density was modelled to be in equilibrium with liquid water at 1 atm. We then performed the 10 ns constant temperature and constant pressure (NPT) dynamics at 1 atm and 300 K, using temperature and barostat coupling constants of 0.1 and 2.0 ps, respectively. A 10 Å cutoff was used for Van der Waals (vdW) and real space electrostatics, with the vdW energies and forces tapered smoothly to zero from 9 Å. All simulations were performed using the LAMMPS 2011 software pakage[30]. The diffusivity of water was calculated using the mean square displacements (MSD) of water based on the Einstein expression. The time correlation function (TCF) formulism was also used to calculate diffusivity, but yielded the same results as MSD for the two-graphene system; therefore, the MSD method was used throughout all systems.

Density functional calculations for water migration. The electronic structure of the system was obtained by first-principles calculations using the SIESTA pseudopotential code[31]. All calculations were carried out using the generalized gradient approximation (GGA-PBE)[32] previously used for modelling graphene-water-SiO_2 substrate interactions[23]. A full optimization of the atomic positions was performed. During optimization, the electronic ground state was consistently found using norm-conserving pseudo-potentials for cores, a

double-ζ plus polarization basis of the localized orbitals for silicon, carbon, and oxygen, and a double-ζ basis for hydrogen. Optimization of the force and total energy was performed with an accuracy of 0.04 eV/Å and 1 meV, respectively. All calculations were carried out with an energy mesh cut-off of 300 Ry and a *k*-point mesh of 4×4×4 in the Monkhorst-Park scheme[33]. Modeling of the graphene over mica was performed for a graphene 3×3 supercell containing 32 carbon atoms over 6 layers of α-SiO_2 substrate containing 25 silicon and 50 oxygen atoms. As in previous work[23], the small mismatch between the lattices of the graphene supercell and mica substrate was neglected. We considered the structural confinement effects of mica on water but not the electrostatic or chemical effects.

References

1. Zhu, Y. & Granick, S. Viscosity of interfacial water. *Phys. Rev. Lett.* **87**, 096104 (2001)
2. Jinesh K. B. & Frenke J. W. M. Capillary Condensation in Atomic Scale Friction: How Water Acts like a Glue. *Phys. Rev. Lett.* **96**, 166103 (2006)
3. Bluhm, H., Inoue, T. & Salmeron, M. Friction of ice measured using lateral force microscopy. *Phys. Rev. B* **61**,7760 – 7765 (2000)
4. Israelachvili, J. N. *Intermolecular and Surface Forces* (Academic Press, 1992)
5. Han, S., Choi, M. Y., Kumar, P. & Stanley, H. E. Phase transitions in confined water nanofilms. *Nat. Phys.* **6**, 685-689 (2010)
6. Somorjai, G. A., Frei, H. & Park, J. Y. Advancing the Frontiers in Nanocatalysis, Biointerfaces, and Renewable Energy Conversion by Innovations of Surface Techniques. *J. Am. Chem. Soc.* **131**, 16589-16605 (2009)
7. Pascal, T. A., Goddard, W. A. & Jung, Y. Entropy and the driving force for the filling of carbon nanotubes with water. *Proc. Natl. Acad. Sci.* **108**, 11794-11798 (2011)
8. Takaiwa, D., Hatano, I., Koga, K. & Tanaka, H., Phase diagram of water in carbon nanotubes. *Proc. Natl. Acad. Sci*. **8**, 39-43 (2010)
9. Nevin, N. *et al.* Observation of Water Confined in Nanometer Channels of Closed Carbon Nanotubes. *Nano Lett.* **4**, 2237-2243 (2004)
10. Cicero, G., Grossman, J. C., Schwegler, E., Gygi, F. & Galli, G. Water Confined in Nanotubes and between Graphene Sheets: A First Principle Study. *J. Am. Chem. Soc.* **130**, 1871-1878 (2008)
11. Douwe, J. B., *et al.* Theory and simulations of water flow through carbon nanotubes: prospects and pitfalls. *J. Phys.: Condens. Matter* **23,** 184110 (2011)
12. John A. T. & Alan J. H. M. Water Flow in Carbon Nanotubes: Transition to Subcontinuum Transport. *Phys. Rev. Lett.* **102**, 184502 (2009)
13. Park, J. H. & Aluru, N. R. Diffusion of water submonolayers on hydrophilic surfaces. *Appl. Phys. Lett.* **93**, 253104 (2008)
14. Park, J. H. & Aluru, N. R. Ordering-Induced Fast Diffusion of Nanoscale Water Film on Graphene. *J. Phys. Chem. C* **114**, 2595-2599 (2010)
15. Uthaisar, C. & Barone, V. Edge Effects on the Characteristics of Li Diffusion in Graphene. *Nano Lett.* **10**, 2838-3842 (2010)

16. Yang, M. *et al.* Manipulating absorption and diffusion of H atom on graphene by mechanical strain. *AIP Adv.* **1**, 032109 (2011)
17. Xu, K., Cao, P. & Heath, J. R. Graphene visualizes the first water adlayers on mica at ambient conditions. *Science* **329**, 1188-1191 (2010)
18. Lui, C. H., Liu, L., Mak, K. F., Flynn, G. W. & Heinz, T. F. Ultraflat graphene. *Nature* **462**, 339-341 (2009)
19. Rudenko, A. N., Keil, F. J., Katsnelson, M. I. & Lichtenstein, A. I. Graphene adhesion on mica: Role of surface morphology. *Phys. Rev. B.* **83**, 045409 (2011)
20. Schirmeisen, A., Jansen, L., Fuchs, H. Tip-jump statistics of stick-slip friction, *Phys. Rev. B* **71**, 245403 (2005)
21. Hu, J., Xiao, X.-D., Ogletree, D. F. & Salmeron, M. Imaging the Condensation and Evaporation of Molecularly Thin Films of Water with Nanometer Resolution. *Science* **268**, 265-269 (1995)
22. Wehling, T. O, Lichtenstein, A. I. and Katsnelson, M. I. First-principles studies of water adsorption on graphene: The role of the substrate. *Appl. Phys. Lett.* **93**, 202110 (2008)
23. Li, T.-D., Gao, J., Szoszkiewicz, R., Landman, U. and Riedo, E. Structured and viscous water in subnanometer gaps. *Phys. Rev. Lett.* **75**, 115415 (2007)
24. Paliy, M., Braun, O.M. and Consta, S. The Friction properties of an ultrathin confined water film. *Tribo. Lett.* **23**, 7-14 (2006)
25. Wang, C. *et al*. Stable liquid droplet on a water monolayer formed at room temperature on ionic model substrates, *Phys. Rev. Lett.* **103**, 137801 (2009)
26. Leng, Y. and Cummings, P. T. Fluidity of Hydration layers nanoconfined between mica surfaces, *Phys. Rev. Lett*. **94**, 026101 (2005)
27. Kimmel, G. A. *et al.* No Confinement Needed: Observation of a Metastable Hydrophobic Wetting Two-Layer ice on Graphene. *J. Am. Chem. Soc.* **131**, 12838-12844 (2009)
28. Liu, Y.-C. *et al.* Diffusion dynamics of water controlled by topology of potential energy surface inside carbon nanotubes. *Phys. Rev. B* **77**, 12438 (2008)
29. Heinz, H. *et al.* Force Field for Mica-Type Silicates and Dynamics of Octadecylammonium Chains Grafted to Montmorillonite. *Chem. Mater.* **17**, 5658-5669 (2005)
30. Plimpton, S. Fast Parallel Algorithms for Short-Range Molecular Dynamics. *J. Comput. Phys.* **117**, 1-19 (1995)
31. Soler, J. M. *et al.* The SIESTA method for *ab initio* order-*N* materials simulation. *J. Phys.: Condens. Matter* **14**, 2745-2779 (2002)
32. Perdew, J. P., Burke, K. & Ernzerhof, M. Generalized Gradient Approximation Made Simple. *Phys. Rev. Lett.* **77**, 3865 (1996)
33. Monkhorst, H. J. & Park, J. D. Special points for Brillouin-zone integrations. *Phys. Rev. B* **13**, 5188 (1976)

Acknowledgements

This work was supported by the National Research Laboratory (NRL) Program (Grant No. 2008-0060004), World Class University (WCU) Programs (Grant No. R31-2008-000-10057-0 and Grant No. R31-2008-000-10055-0), Midcareer Researcher Program (No. 2011-0017605), Basic Science Research Programs (KRF-2008-314-C00111, 2010-0015035, and

2012R1A2A1A01009249), Nano × Material Technology Development Program (2011-0030228), Center for Advanced Soft Electronics under the Global Frontier Research Program (No. 2011-0031630, 2011-0031640, and 2011-0031660), and Quantum Metamaterials Research Center (Grant No. R11-2008-053-03002-0) through the National Research Foundation of Korea (NRF) funded by the Ministry of Education, Science and Technology (MEST). Y.-W.S. was supported in part by the Center for Advanced Soft Electronics (Grant No. 2011-0031640) of the MEST. MBS was supported by the Office of Basic Energy Sciences, Division of Materials Sciences and Engineering of the US DOE under Contract No. DE-AC02-05CH11231. J.-S.K. was supported by a Hi Seoul Science/Humanities Fellowship from the Seoul Scholarship Foundation. Y.J. acknowledges the support from EEWS Initiative and NRF-Korea (2010-0023018). Calculations were supported by CAC of KIAS and KISTI supercomputing center.

Author contribution state

J.-S.K. and B.H.P. planned the projects; J.-S.K., J.S.C., B.H.P., J.Y.P., and M.S. designed the experiments; J.-S.K., J.S.C., and M.J.L. carried out the AFM measurements; D.Y. and H.C. obtained and analyzed the micro-Raman spectroscopy data; Y.-W.S., D.B., J.-N.Y., and Y.J. performed and analyzed the calculations; J.-S.K., B.H.P., H.C., Y.-W.S., Y.J., J.Y.P., and M.S. interpreted the results; all authors discussed the results and commented on the manuscript.

Competing financial interests

The authors declare no competing financial interests.

Supplementary Information

Between Scylla and Charybdis: Hydrophobic Graphene-Guided Water Diffusion on Hydrophilic Substrate

Jin-Soo Kim[1], Jin Sik Choi[1], Mi Jung Lee[2], Bae Ho Park[2,*], Danil Bukhvalov[3], Young-Woo Son[3], Duhee Yoon[4], Hyeonsik Cheong[5], Jun-Nyeong Yun[6], Yousung Jung[6], Jeong Young Park[6,**], and Miquel Salmeron[7]

[1]Creative Research Center for Graphene Electronics, Electronics and Telecommunications Research Institute (ETRI), Daejeon 305-700, Korea.
[2]Division of Quantum Phases and Devices, Department of Physics, Konkuk University, Seoul 143-701, Korea.
[3]Korea Institute for Advanced Study, Seoul 130-722, Korea.
[4]Electrical Engineering Division, Cambridge University, Cambridge, CB3 0FA, UK
[5]Department of Physics, Sogang University, Seoul 121-742, Korea.
[6]Graduate School of EEWS, NanoCentury KI, Korea Advanced Institute of Science and Technology (KAIST), Daejeon 305-701, Korea.
[7]Materials Science Division, Lawrence Berkeley National Laboratory, Berkeley, CA 94720, USA.
[*]email: baehpark@konkuk.ac.kr; **email: jeongypark@kaist.ac.kr

I. Graphene exfoliated on a SiO_2 substrate

Figure S1 shows an AFM topographic image near the edge of graphene mechanically exfoliated on a SiO_2 substrate under high humidity of ~ 40%. The height variation of graphene (σ = 117.7 pm) is larger than that of SiO_2 (σ = 88.1 pm), probably due to intercalated water between the graphene and SiO_2, in contrast to Ref. 18 where the sample is made in a glove box maintained at low humidity. The average height of the graphene over the SiO_2 substrate is 1.34 ± 0.05 nm, which is larger than the layer spacing in graphite (0.34 nm), since intercalated water may elevate the graphene layer. However, the AFM topographic image in Fig. S1(a) does not exhibit flat layers of water that fill most of the interior of the graphene overlayer on the mica substrate. The absence of an initial crystalline and

epitaxially-oriented water layer on the SiO_2 substrate may result from the amorphous surface structure of the substrate.

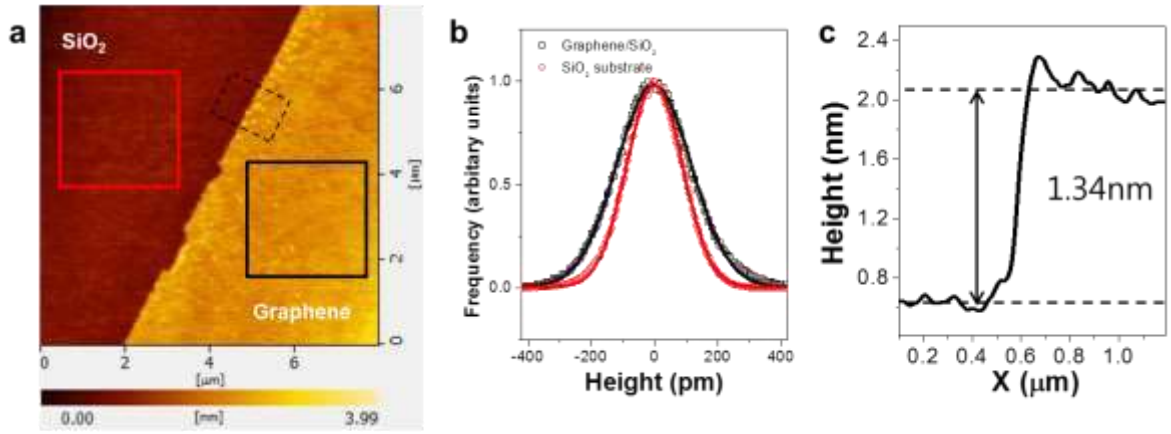

Figure S1. Surface structure of graphene exfoliated on SiO_2. (**a**) AFM topographic image near the edge of graphene on a SiO_2 substrate. (**b**) Height histograms for graphene on SiO_2 (open black square) and a bare SiO_2 substrate (open red circle). The data, obtained inside the black and red squares in image (**a**), are fitted by Gaussian distributions (solid lines) with standard deviations (σ) of 117.7 pm and 88.1 pm, respectively. (**c**) Average step height profiles measured for the black dashed square in (**a**).

II. Raman characterization of graphenes

Figure S2 shows Raman spectra of region I before and after high humidity treatment, revealing no noticeable difference. This indicates that the bilayer graphene is preserved after the high humidity treatment. The decrease of the I_{2D}/I_G ratio after the high humidity treatment could be induced by a change in the dielectric surface under the graphene layer[S1]. These results also support that water diffused into the interface between the graphene and mica.

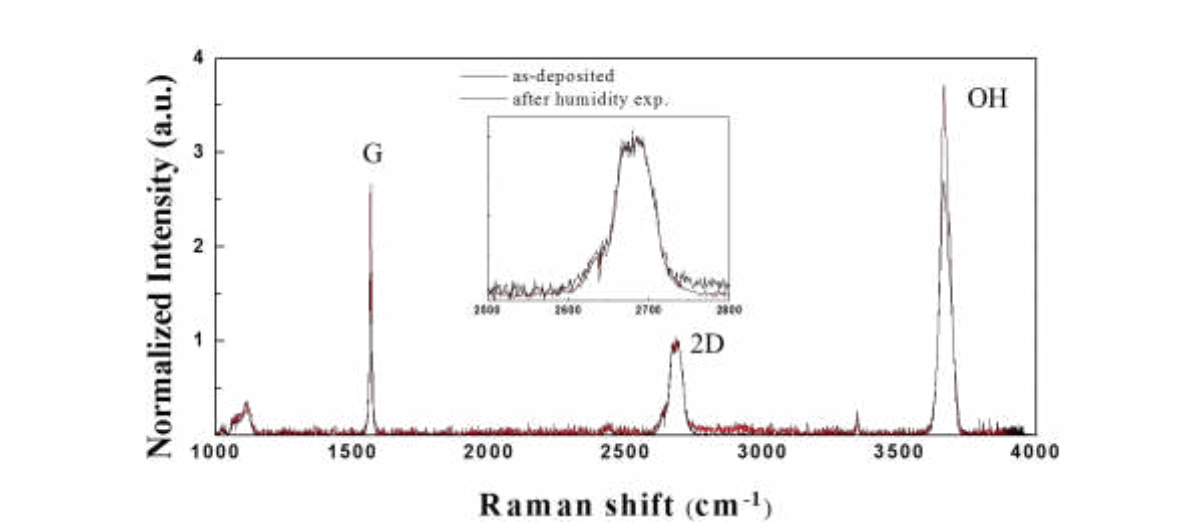

Figure S2. Spatially resolved Raman spectra of region I before and after the high humidity treatment. The measured signal was normalized to the 2D peak intensity. The inset shows the expanded Raman spectra near the 2D peak position. No noticeable difference of peak position and shape is found in the Raman spectra, while the intensity of the G and OH peaks increases after the high humidity treatment.

III. Stacking order of graphene layers

Figure S3 shows stacking structures of graphene with an AB stacking order and an ABC stacking order. Blue lines denote the zigzag directions of the top-most graphene layer. This shows that the zigzag direction of the upper graphene layer is the same as that of the lower graphene layer, regardless of the stacking order of the graphite.

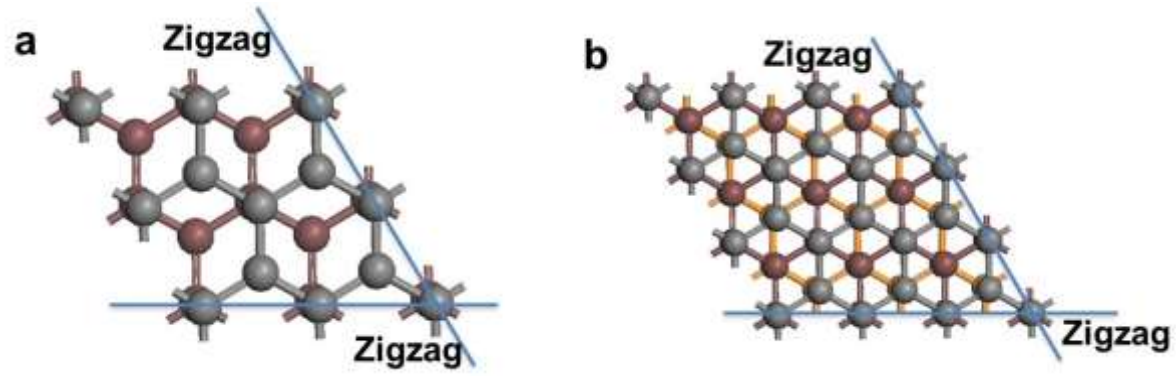

Figure S3. Graphene stacking structures. (**a**) An AB stacking order. (**b**) An ABC stacking order. Blue lines denote the zigzag directions of the top-most graphene layer. They are identical to those of the bottom graphene layers in both the AB and ABC stacking orders.

IV. Water stability between graphene and mica

The stability of the confined water between the graphene and mica was investigated by changing the temperature and/or the water vapor pressure. While both layered and stripe structures (Fig. S4(a)) are clearly observed at room temperature and normal humidity, the stripe structure disappears, giving rise to numerous droplets when the chamber is evacuated to 10^{-5} atm, as shown in Fig. S4(b). Given the measurement procedure, it seems that the transformation from the stripe structure to droplets takes place in one hour. At a temperature of -50 °C and pressure of 10^{-5} atm, the layered structure is still observed, but the water droplets become craggy (Fig. S4(c)).

The transformation of the stripe pattern into a collection of droplets may be the result of the evolution from a flat wetting film to a 3D non-wetting structure, indicating weak interaction between the stripe pattern and the hydrophilic mica substrate. By decreasing the temperature, the droplets solidify, losing their circular dome-shape and adopting irregular shapes, as shown in Fig. S4(c). In contrast, the flat, molecularly-thin layered structure is unaffected by lowering the temperature and pressure (Figs. S4(b) and S4(c)), implying that it is strongly bound to the hydrophilic mica substrate.

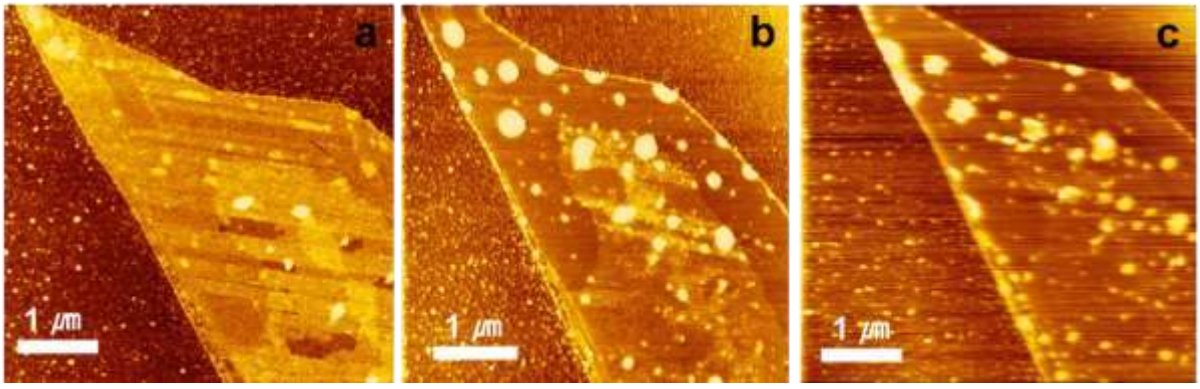

Figure S4. Changes induced by decreasing pressure and temperature. Topographic images of graphene on mica after high humidity exposure, measured at (**a**) room temperature and normal pressure, (**b**) room temperature and 10^{-5} atm, and (**c**) -50 °C and 10^{-5} atm. The stripe structure in (**a**) collapses and gives rise to spherical cap droplets in (**b**), while the layered water remains. After further cooling, the droplets adopt irregular geometric shapes, indicative of solidification.

V. Confined water molecules

Figure S5 exhibits the atomic models for water molecules confined in nanostructures that are used for molecular dynamics calculations. The diffusional anisotropy of water between the two mica surfaces, defined as an average of the relative diffusivities of water along the three unique mutually-perpendicular axes, is 1.04, almost 2D-isotropic, unlike water confined by graphene surfaces whose dynamics is highly directional. CNTs also reveal anisotropic diffusivity of water: remarkably, a 4.5-fold increase in water diffusivity along the zigzag direction, compared to the armchair direction.

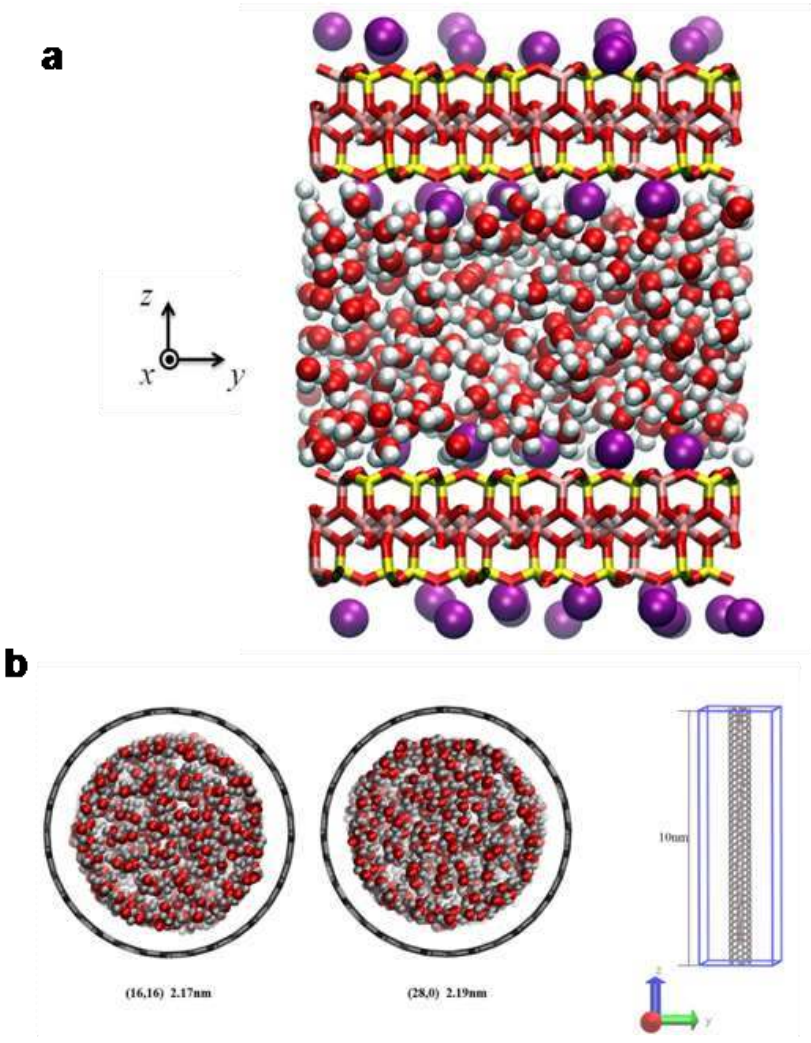

Figure S5. Confined water molecules. Atomic structures of water molecules confined between (**a**) mica and mica, and (**b**) in armchair (16,16) or zigzag (28,0) CNTs.

VI. Atomic models for density functional calculations

Figure S6 exhibits projected atomic structures of water intercalated between a graphene monolayer and a mica substrate. In our density functional calculations, there is no competition between the ice-graphene and ice-mica interactions. There is only competition between the internal interactions in ice and ice-mica interactions; the internal interactions are superior to ice-mica interactions. The hexagonal structure of graphene is the matrix for the transformation of water from structures connected with mica to the very energetically-favorable hexagonal ice. So, the interaction between water and the graphene overlayer was considered significant and the dependence of water diffusivity on the crystallographic orientation of graphene was investigated. The mica substrate is introduced in order to make our calculations as realistic as possible, and to study the competition between internal interactions in ice and ice–mica interactions and the role of mica as a confining well.

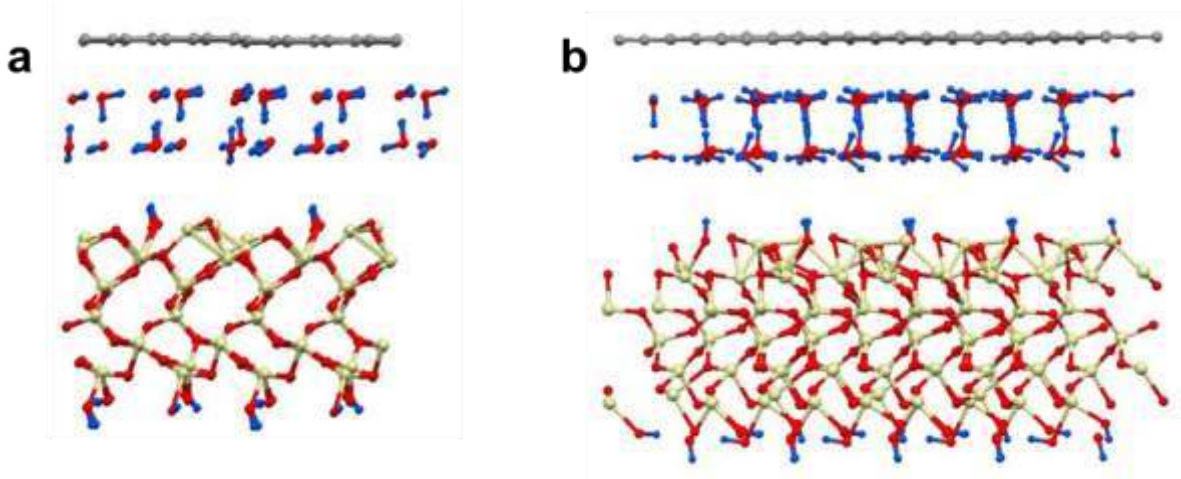

Figure S6. Projections of atomic models for density functional calculations. Atomic models of water intercalated between a graphene monolayer and a mica substrate projected (**a**) along the zigzag direction of graphene and (**b**) along the armchair direction of graphene.

Table I. The comparison of self-diffusivity (D_{tot}) in bulk water and our model.

Model	Self-Diffusivity D_{tot} (cm^2/s)
Bulk water[S2]	2.299E-05
Bulk water (SPC/E)	2.408E-05
25.59x27.06x14 graphene/graphene	1.394E-05
25.96x27.05x14 graphene/mica	1.299E-05
25.96x27.05x14 mica/mica	1.070E-05

References

S1. Yoon, D. *et al.,* Interference effect on Raman spectrum of graphene on SiO_2/Si. *Phys. Rev. B* **80**, 125422 (2009)

S2. Holz, M., Heil, S.R., Sacco, A., Temperature-dependent self-diffusion coefficients of water and six selected molecular liquids for calibration in accurate 1H NMR PFG Measurements, *Phys. Chem. Chem. Phys*. **2**, 4740–4742 (2000)